Editors' Suggestion   Featured in Physics

First Direct Measurements of Superheavy-Element Mass Numbers

J. M. Gates,[1,*] G. K. Pang,[1] J. L. Pore,[1] K. E. Gregorich,[1] J. T. Kwarsick,[1,2] G. Savard,[3,4] N. E. Esker,[5] M. Kireeff Covo,[1]
M. J. Mogannam,[1] J. C. Batchelder,[2] D. L. Bleuel,[6] R. M. Clark,[1] H. L. Crawford,[1] P. Fallon,[1] K. K. Hubbard,[1,2]
A. M. Hurst,[2] I. T. Kolaja,[2] A. O. Macchiavelli,[1] C. Morse,[1] R. Orford,[3,7] L. Phair,[1] and M. A. Stoyer[6]

[1]*Lawrence Berkeley National Laboratory, Berkeley, California 94720, USA*
[2]*University of California, Berkeley, California 94720, USA*
[3]*Argonne National Laboratory, Argonne, Illinois 60439, USA*
[4]*University of Chicago, Chicago, Illinois 60637, USA*
[5]*TRIUMF, Vancouver, British Columbia V6T 2A3, Canada*
[6]*Lawrence Livermore National Laboratory, Livermore, California 94550, USA*
[7]*McGill University, Montreal, Québec H3A 0G4, Canada*

An experiment was performed at Lawrence Berkeley National Laboratory's 88-in. Cyclotron to determine the mass number of a superheavy element. The measurement resulted in the observation of two α-decay chains, produced via the ^{243}Am(^{48}Ca, xn)$^{291-x}$Mc reaction, that were separated by mass-to-charge ratio (A/q) and identified by the combined BGS + FIONA apparatus. One event occurred at $A/q = 284$ and was assigned to ^{284}Nh ($Z = 113$), the α-decay daughter of ^{288}Mc ($Z = 115$), while the second occurred at $A/q = 288$ and was assigned to ^{288}Mc. This experiment represents the first direct measurements of the mass numbers of superheavy elements, confirming previous (indirect) mass-number assignments.

Atoms of superheavy elements (SHE) have been produced at the Joint Institute for Nuclear Research (JINR) in compound-nucleus reactions between ^{48}Ca projectiles and actinide targets (hot fusion reactions) for nearly 20 years [1–3]. During the last several years, SHE production in such hot fusion reactions has been reported from laboratories in the USA [4–6], Germany [7–11], and Japan [12], both confirming and extending the JINR SHE claims. In previous discoveries up to Nh [proton number (Z) 113], mass number (A) and Z assignments were made by observing the α-decay chain of a new element isotope until it decayed into an isotope with well-established Z, A, and decay properties [13]. Unfortunately, all isotopes of SHE produced in ^{48}Ca irradiations of actinide targets have α-decay chains that terminate with the spontaneous fission of a daughter isotope, without decaying through an isotope with well-established Z or A. For these SHE isotopes, presumed Z and A assignments have been made based on (i) decay systematics, (ii) production rate as a function of bombarding energy (excitation functions), (iii) producing the same isotopes using different target materials [cross bombardments, e.g., ^{287}114 produced in the ^{244}Pu(^{48}Ca, $5n$) and ^{242}Pu(^{48}Ca, $3n$) reactions] and (iv) the assumption that deexcitation of the excited compound system through charged particle emission does not occur [2,3,13]. However, these four techniques are indirect and, ultimately, depend on the accuracy of nuclear mass models [14,15]. While it is likely that the suggested Z and A assignments are correct, it is imperative that they are confirmed directly through experiment. The slight, but highly consequential, possibility that the Z and A assignments are systematically wrong would radically alter the interpretation and understanding of nuclear behavior at the high-Z limit of stability, potentially masking unexpected and exotic nuclear phenomena.

In this work, we report on the first direct experimental measurements of the mass number of the SHE isotopes, ^{288}Mc (moscovium, $Z = 115$) and ^{284}Nh (nihonium, $Z = 113$), produced in the ^{243}Am(^{48}Ca, $3n$)^{288}Mc reaction.

Beams of ^{48}Ca^{11+} were produced from enriched-metallic Ca in VENUS (versatile ECR ion source for nuclear science) [16,17] and accelerated through Lawrence Berkeley National Laboratory's (LBNL) 88-in. Cyclotron to laboratory-frame energies of 262 MeV at an average intensity of 6×10^{12} ions/s for a total integrated dose of 1.0×10^{18} ^{48}Ca^{11+} ions. The ^{48}Ca beam passed through a differential pumping section separating the beam line vacuum from the 53-Pa He fill gas inside the Berkeley Gas-Filled Separator (BGS) [18]. Immediately downstream of the differential pumping section, the beam impinged on a rotating (∼30 Hz) target wheel (radius = 3.8 cm) consisting of four arc-shaped ^{243}Am$_2$O$_3$ targets, prepared by electrodeposition of ^{243}Am onto the downstream side of 2.7(1)-μm-thick Ti foils. The average ^{243}Am thickness was 472 μg/cm^2. Additionally, a layer of approximately 100 μg/cm^2 ^{159}Tb was deposited on the upstream side of the Ti foils for production of At isotopes that were used to

calibrate the mass number-to-charge ratio (A/q, where q is the charge state of the ion) measurements, as described below.

Measurement periods alternated between Mc production (8 h) and At calibration (20 min). The Mc (At) ions recoiled out of (through) the targets and were separated from unreacted beam and other nuclear-reaction products in the BGS, as described in previous publications [5,18]. At the BGS focal plane the Mc (At) ions passed through a 2.1-μm Ti foil and into the newly commissioned FIONA apparatus [19]. FIONA (for the identification of nuclide A) consists of a radiofrequency (rf) gas catcher, rf quadrupole (RFQ), RFQ trap, acceleration region, trochoidal spectrometer (mass analyzer), and detector station. A schematic of the BGS + FIONA system is shown in Fig. 1 and the locations of the items are highlighted. Technical aspects of its commissioning and operation will be described elsewhere [20]. FIONA is designed to cool and bunch ions selected by the BGS before transporting them into a low-background area for A/q separation and identification on a tens-of-milliseconds timescale.

Upon entering FIONA, the Mc (At) ions were stopped in 13 kPa of ultrapure He inside the rf gas catcher, with some retaining a positive ionic charge (see Ref. [21] for a discussion of the operation of a gas catcher of similar design). Then rf and dc (direct current) electric field gradients directed the ions toward the exit orifice. Using a reduced ion mobility in He of 20×10^{-4} m^2/(V s), the average drift time through the gas catcher is estimated to be approximately 28 ms. After passing through the gas catcher exit orifice, the ions were radially confined in the segmented RFQ, while the He gas was differentially pumped to a pressure of approximately 30 Pa. An axial dc gradient, applied along the RFQ axis, directed the ions downstream where they were captured in the RFQ trap, which was configured with an axial dc gradient profile to create a three-dimensional ion trap [22]. Differential pumping on this RFQ trap maintained a He pressure of ~2 Pa in this

region. Collisions with the He buffer gas in the trap region cooled the ions to several times thermal energies and confined them to within ~1 mm^3. Every 20 ms the dc voltages on the RFQ trap segments were changed to eject the cooled ions into a region containing acceleration electrodes (including a pulsed drift tube), steering electrodes, and Einzel lenses. The Mc^{1+} and At^{1+} ions were accelerated to 3319 and 4789 eV, respectively.

After acceleration, the ions traveled through a drift region and into an area of low γ and neutron background (separated from the BGS area by a shielding wall), where they were separated by their A/q using the trochoidal spectrometer (mass analyzer) [19]. The trochoidal spectrometer consists of a relatively small flat-field magnet ($l \times w \times h = 50$ cm $\times$ 50 cm $\times$ 8 cm) with a maximum magnetic field of 1.1 T in the downward (gravity) direction and perpendicular to the beam direction. Inside the magnet vacuum chamber, top- and bottom-striped circuit boards with resistor chains created a uniform electric field perpendicular to both the magnetic field and the velocity vector of the entering ions. By suitable choice of the crossed magnetic and electric field strengths, the ions follow trochoidal trajectories [23–27]. The period and beam-direction precession of these trochoids depends on the A/q and is independent of velocity. Thus, A/q separation is based on the trochoid-phase differences of ions with different A/q when they exit the magnetic and electric fields, which results in different exit angles in the plane defined by the beam and electric field directions (dispersive plane). The FIONA A/q separation has been tested extensively with ions produced at the 88-in. Cyclotron and with ^{216}Po^{1+} ions from a ^{232}U source that emanated ^{220}Rn. The trochoidal spectrometer was run using two-loop trajectories with 15-cm amplitudes to optimize both physical separation of adjacent masses and transportation efficiency.

After exiting the trochoidal spectrometer, the ions were implanted in a single-sided, 16-strip resistive readout (2D-position-sensitive) detector at the FIONA focal plane, which is approximately 75 cm downstream of the exit point of the trochoidal spectrometer (focal-plane detector). The focal-plane detector was surrounded by a tunnel of our 16-strip single-sided silicon detectors (upstream detectors), forming a combined detector array in the shape of a five-sided cube. The focal-plane detector and four upstream detectors each have an active area of 58×58 mm and are divided into 3.625-mm wide strips. Energies of events in the FIONA detector were calibrated using a source containing ^{239}Pu ($E_\alpha = 5156.59$ keV, with a branching ratio Br$_\alpha = 73.3\%$), ^{241}Am ($E_\alpha = 5485.56$ keV, Br$_\alpha = 84.5\%$), and ^{244}Cm ($E_\alpha = 5804.82$ keV, Br$_\alpha = 76.4\%$). The positions of events in the dispersive axis of the focal-plane detector were determined by resistive charge division, while the nondispersive position was given by the strip number in which that event was detected. The data acquisition was triggered by either an event in the focal
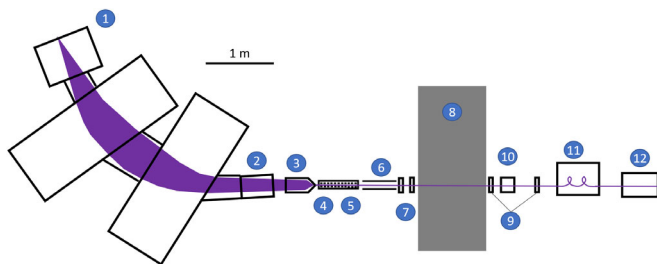

FIG. 1.   Schematic of BGS + FIONA with the labels indicating the positions of 1. BGS, 2. BGS focal plane detector, 3. gas catcher, 4. RFQ, 5. RFQ trap, 6. acceleration region, 7. focusing element, horizontal and vertical steerers, 8. shielding wall, 9. focusing element, horizontal and vertical steerers, 10. C2 detector, 11. trochoid spectrometer, and 12. FIONA focal-plane detector. The purple shaded area or line represents the beam image of ^{288}Mc traveling through the BGS and FIONA.

plane or upstream silicon detectors with an energy above approximately 1 MeV.

In this experiment, the ion acceleration, focusing, steering, and trochoidal spectrometer were calibrated with $^{198-201}$At^{1+} ions to optimize efficiency and A/q resolution. A subset of experimental data from the calibration runs is shown in Fig. 2 (top, mid). At the FIONA focal plane, the A/q dispersion is approximately 20-mm-per-percentage difference in A/q. The mass resolving power, with separation of adjacent masses at the full-width-at-tenth-maximum level, is $(A/q)/\Delta(A/q) = 250$. The typical At^{1+} transport and detection efficiency from the BGS focal plane, through FIONA, and to the FIONA focal-plane detector was 14(2)% and was determined by comparing the measured rate of At at the BGS focal-plane detector to the measured rate of At^{1+} at the FIONA focal-plane detector.

Scaling of FIONA from the calibration $(A/q)_{\text{calib}}$ value, obtained with At^{1+} ions, to the desired $(A/q)_{\text{new}}$ value for Mc^{1+} ions was carried out by scaling the acceleration potentials such that ions corresponding to $(A/q)_{\text{new}}$ have the same magnetic rigidity as those with $(A/q)_{\text{calib}}$. Therefore, no change to the trochoidal spectrometer magnet was required, avoiding hysteresis effects. The voltages on the RFQ trap ejection electrodes, steering and focusing electrodes, and the electrodes inside the trochoidal
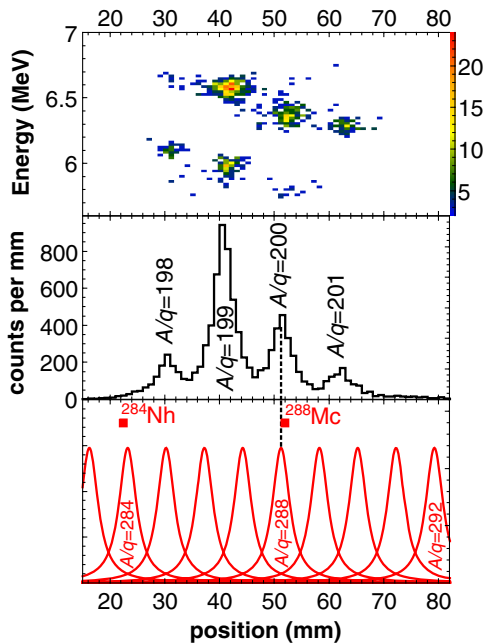
spectrometer were scaled by $(A/q)_{\text{calib}}/(A/q)_{\text{new}}$ to match the electric rigidity of the ions with $(A/q)_{\text{new}}$, while the time between releasing the ions from the RFQ trap and pulsing the drift tube was scaled by $(A/q)_{\text{new}}/(A/q)_{\text{calib}}$. In this way, the Mc^{1+} ions with $(A/q)_{\text{new}}$ then take exactly the same trajectories as the calibration At^{1+} ions with $(A/q)_{\text{calib}}$. During the FIONA commissioning, the calibration procedure was tested by scaling between ions of various masses and charge states, for example, ^{254}No^{2+}, ^{255}Lr^{2+}, ^{151}Ho^{1+}, ^{200}At^{1+}, ^{208}Fr^{1+}, ^{216}Po^{1+}, ^{245}Fm^{1+}, ^{254}No^{1+}, and ^{255}Lr^{1+}. The results of these measurements are shown in Fig. 3. Based on these results, the accuracy of the A/q calibration procedure results in a ± 0.5-mm A/q calibration error in FIONA focal-plane positions.

Based on a comparison of the theoretic second ionization potential of Mc [28] to the known second ionization potentials of Fm, No, Lr, At, Po, and Fr, and the experimental ratio of $1 + /2+$ ions observed at the exit of the acceleration region [Fig. 1 (10)], the Mc ions are expected to retain a 1^+ charge state. Therefore, the trochoidal spectrometer was tuned such that only ions with $283 < A/q < 290$ would reach the detector during the Mc measurement runs. Given this, we do not expect to observe decays from transfer reaction products in the detector.

Decay chains potentially originating from Mc were identified using correlations consisting of two or more α-like events [$9 < E_\alpha(\text{MeV}) < 10.6$] detected within 60 s, with at least one α-like event occurring in the focal-plane detector within the same nondispersive (y position)

FIG. 2. (top) Experimental data from the At^{1+} calibration run showing the α-particle energies versus the positions they were observed in the focal plane detector; (middle) experimental data from the At^{1+} calibration runs taken before and after each event was observed and showing the A/q separation; (bottom) expected location of $A/q = 283$–292 mass peaks at the FIONA focal-plane detector. The locations of the two observed events are shown by the squares.
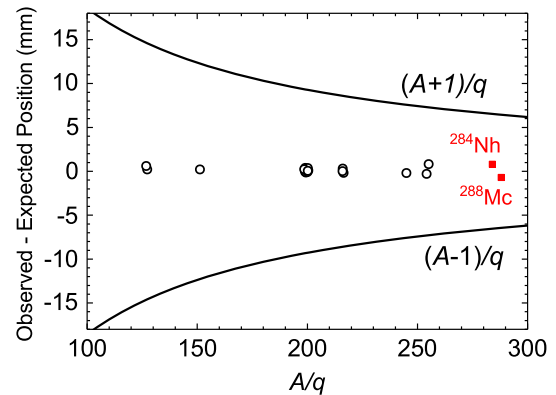

FIG. 3. Deviation of the observed focal plane position from the expected position (after scaling) as a function of A/q. The open circles correspond to the results for known isotopes, ^{254}No^{2+}, ^{255}Lr^{2+}, ^{151}Ho^{1+}, ^{200}At^{1+}, ^{208}Fr^{1+}, ^{216}Po^{1+}, ^{245}Fm^{1+}, ^{254}No^{1+}, and ^{255}Lr^{1+} and the error bars are smaller than the symbols. The red squares correspond to the two events of ^{284}Nh and ^{288}Mc discussed in the text. The lines represent the expected centroids of masses with $(A \pm 1)/q$ from the scaled mass. From the commissioning measurements, the observed position agrees within ± 0.5 mm of the predicted (scaled) position, giving a position uncertainty that is small compared to the separation between adjacent mass numbers.

range (strips 6–9) as the calibration ions. During the Mc measurement periods α-like events were observed from background from long-lived implants from previous experiments. The average rate of α-like events was 2.9×10^{-6} Hz in the focal plane and 3.9×10^{-5} Hz in the upstream detectors. During 1.7×10^5 s of running time, six of these α-like events were observed in the focal-plane detector, while 81 were observed in the upstream detectors. Consequently, we expect 0.03 random correlations between pairs of α-like events, with at least one α particle detected in the focal-plane detector. The expected number of random correlations between three or more unrelated α-like events is more than 3 orders of magnitude smaller. If one requires that the α energies closely resemble the energies along the ^{288}Mc decay chain, then the number of expected random correlations is further decreased. Given these random rates, we are confident that the events reported here are not random correlations of unrelated events.

The ^{243}Am$(^{48}$Ca, $xn)$ reaction has been shown to produce three distinct α-decay chains, which have been associated with the different Mc isotopes, $A = 287$, 288, and 289 [5,11,29]. Based on previous experiments [5] and the beam energy used in this measurement, we would expect to observe α particles originating from the presumed ^{288}Mc decay chain, which consists of five high-energy α decays with the decay properties shown in Fig. 4 (left) [5,11,29]. The efficiency for identification of Mc decay chains in the five-sided silicon detector box was modeled using Monte Carlo techniques. With an acceleration potential

of 3.319 kV, the Mc^{1+} implantation depth in the FIONA focal-plane detector is only ≈ 10 nm and the energy imparted into the detector is below the detector threshold. Therefore, we do not record an "implantation" signal and the information regarding the lifetime of the first α decay in each chain is lost. Additionally, the recoil energy imparted to the α-decay daughter is sufficient to eject the daughter from the focal-plane detector and into one of the upstream detectors (or to allow escape through the open end of the detector box), depending on the direction of the emitted α particle. The Monte Carlo simulation modeled the position, depth, and straggling of Mc ions entering the focal-plane detector. For each α-decaying chain member, the isotropic emission of α particles with known energy and the recoil of the α-decay daughter were modeled. If detection of at least two (three) of the five α decay chain members is required for ^{288}Mc identification the efficiency is 93% (85%). The Monte Carlo simulation was also repeated for the four-member ^{284}Nh decay chains (under the scenario that the α decay of the parent ^{288}Mc occurred in the gas catcher), resulting in an efficiency of 88% (69%) for detecting at least two (three) of the four α-decay chain members. The simulations also show that the position of the first α decay detected in the focal-plane detector is always the implantation site of the initial ion.

Two decay chains were observed as shown in Fig. 4 (right). The first decay chain consisted of an α particle with $E_\alpha = 9.93(6)$ MeV followed 34.376 s later by an α particle with $E_\alpha = 9.19(6)$ MeV. The energy of the first observed α particle is consistent with the energy of the α decay that is typically assigned to ^{284}Nh ($E_\alpha = 9.98$ MeV, $t_{1/2} = 0.94$ s), while the energy and lifetime of the second α particle corresponds to the known decay properties of the presumed ^{272}Bh ($E_\alpha = 9.08$ MeV, $t_{1/2} = 11.0$ s). This decay chain was detected at a dispersive (x) position of 22.4 mm, near the expected peak of the $A/q = 284$ distribution ($x = 23.2$ mm), as shown in Fig. 2 (bottom). Given that we estimate the residence time in the gas catcher to be approximately 28 ms (see earlier discussion), while the half-life of ^{288}Mc is approximately 160 ms, we expect at least 10% of the Mc events to α decay inside the gas catcher. There are also other processes which can increase the Nh:Mc ratio exiting the gas catcher, such as a neutral Mc α decaying to produce a charged Nh. The observed α-particle energies, lifetimes, and position are then all consistent with the interpretation of this event as arising from a ^{288}Mc ion α decaying inside the gas catcher to the detected ^{284}Nh.

A second observed decay chain consisted of four α particles, detected within 20 s, and is also shown in Fig. 4 (right). The energies and lifetimes of the observed α particles are consistent with the properties currently assigned to the isotopes ^{288}Mc, ^{280}Rg, ^{276}Mt, and ^{272}Bh. The first three α particles were observed in the upstream detectors, with the fourth α particle observed in the focal-
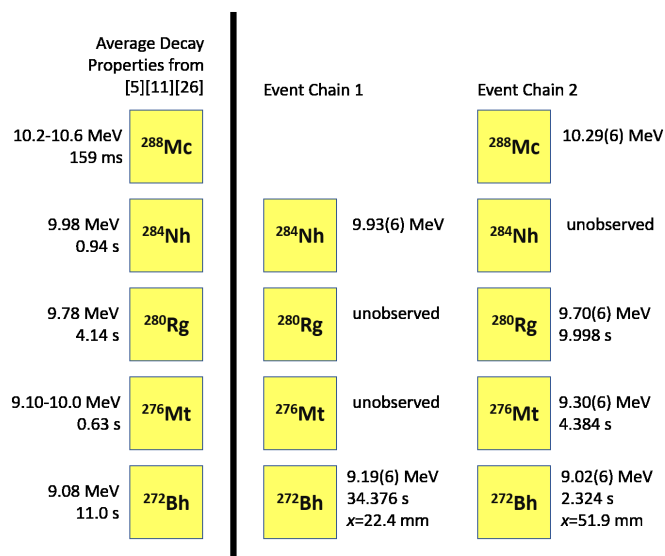

FIG. 4.   (left) Average of known decay properties assigned to ^{288}Mc and its daughters [5,11,29]; (right) details of decay chains detected at the FIONA focal plane. Unobserved decays within each decay chain are indicated as "unobserved" and are assumed to have been emitted out of the open end of the detector array. The x position of decays observed in the focal-plane detector is also given.

plane detector at a position of 51.9 mm, near the peak of the expected $A/q = 288$ mass distribution ($x = 51.2$ mm), as shown in Fig. 2 (bottom).

Assuming (i) a ^{288}Mc production cross section of 8.5 pb [29], (ii) the Mc^{1+} transmission efficiency is the same as the At^{1+} transmission efficiency and (iii) the ^{243}Am targets were not damaged during irradiation, then we would have expected 5.2 events and saw 2. The probability of seeing two or less events when you expect 5.2 is 11%.

To determine the likelihood that these decay chains originated from ^{288}Mc (and its daughter ^{284}Nh) as opposed to neighboring isotopes, A/q calibrations with $^{198-201}$At were measured before and after the Mc and Nh events to determine the A/q peak centroids, Lorentzian peak width, and A/q dispersion. These parameters were then used to predict the peak shapes and positions for SHE ions. The probabilities that the two-member event chain (first event) corresponds to the implantation of an ion with $A/q = 285$, 284, or 283 are 13%, 81%, and 7%, respectively. For the four-member event chain (second event) the probabilities for $A/q = 289$, 288, or 287 are 10%, 83%, and 7%, respectively. Previous studies [5,11,29] have shown that decay chains originating from this target-projectile combination can be sorted into three groups, each with distinct decay properties [29,30]. Both events presented in this work have α-particle energies and lifetimes that are associated with the decay chains that have been previously assigned to ^{288}Mc—which proceed through the five-member α-decay chain shown in Fig. 4 (left). Accordingly, we have assumed that these two event chains originate from the same isotope, that which has been assigned to ^{288}Mc. Applying the constraint that the detected focal plane positions differ by four A/q units, the combined implantation assignment as $A/q = 288$ and 284 has a confidence level of 97.6%. Accordingly, we assign these two event chains to the production and decay of ^{288}Mc.

To assess the effect of uncertainties on our A/q assignment confidence level, a Monte Carlo maximum likelihood calculation was carried out. Uncertainties in the At peak centroids, Lorentzian peak widths, and the A/q dispersion were determined from fits to the experimental At A/q spectrum shown in Fig. 2 (middle). For each of the 10^4 Monte Carlo trials, the ^{200}At centroid, peak width, and dispersion were sampled from the normal distributions determined from the fits. With the constraint that the A/q of the first member of the 4-α event chain is four units larger than the first member of the 2-α chain, the ensemble of properly normalized likelihood probabilities for the $A/q = 288$ and 284 assignments has a narrow distribution with a median likelihood of 97.2%. This shows that the uncertainties have little effect on the A/q assignment confidence level.

In this Letter, we have reported the first experimental determination of the mass numbers of superheavy-element isotopes. With few exceptions [30], the data obtained

from excitation functions, decay systematic, and cross bombardments indicate that the SHE assignments form a contiguous group in Z and A, with correct *relative* mass numbers. If one accepts this premise, our direct experimental measurement of the mass numbers of ^{288}Mc and ^{284}Nh anchor most of the previously reported SHE A assignments, thus finally confirming that most of the mass numbers suggested for other superheavy-element isotopes are correct.

---

* jmgates@lbl.gov

[1] Yu. Ts. Oganessian, J. Phys. G **34**, R165 (2007).
[2] Yu. Ts. Oganessian and V. K. Utyonkov, Rep. Prog. Phys. **78**, 036301 (2015).
[3] Yu. Ts. Oganessian and V. K. Utyonkov, Nucl. Phys. **A944**, 62 (2015).
[4] P. A. Ellison et al., Phys. Rev. Lett. **105**, 182701 (2010).
[5] J. M. Gates et al., Phys. Rev. C **92**, 021301 (2015).
[6] L. Stavsetra, K. E. Gregorich, J. Dvorak, P. A. Ellison, I. Dragojevic, M. A. Garcia, and H. Nitsche, Phys. Rev. Lett. **103**, 132502 (2009).
[7] Ch. E. Düllmann et al., Phys. Rev. Lett. **104**, 252701 (2010).
[8] S. Hofmann et al., Eur. Phys. J. A **32**, 251 (2007).
[9] S. Hofmann et al., Eur. Phys. J. A **48**, 62 (2012).
[10] J. Khuyagbaatar et al., Phys. Rev. Lett. **112**, 172501 (2014).
[11] D. Rudolph et al., Phys. Rev. Lett. **111**, 112502 (2013).
[12] D. Kaji et al., J. Phys. Soc. Jpn. **86**, 034201 (2017).
[13] K. Gregorich, EPJ Web Conf. **131**, 06002 (2016).
[14] G. Audi, M. Wang, A. H. Wapstra, F. G. Kondev, M. MacCormick, X. Xu, and B. Pfeiffer, Chin. Phys. C **36**, 1287 (2012).
[15] M. Wang, G. Audi, A. H. Wapstra, F. G. Kondev, M. MacCormick, X. Xu, and B. Pfeiffer, Chin. Phys. C **36**, 1603 (2012).
[16] D. Leitner, C. M. Lyneis, T. Loew, D. S. Todd, S. Virostek, and O. Tarvainen, Rev. Sci. Instrum. **77**, 03A302 (2006).

[17] C. M. Lyneis, D. Leitner, M. Leitner, C. Taylor, and S. Abbot, Rev. Sci. Instrum. **81**, 02A201 (2010).

[18] K. E. Gregorich, Nucl. Instrum. Methods Phys. Res., Sect. A **711**, 47 (2013).

[19] J. M. Gates, EPJ Web Conf. **131**, 08003 (2016).

[20] J. M. Gates, K. E. Gregorich, N. E. Esker, G. K. Pang, J. L. Pore, J. T. Kwarsick, and G. Savard (to be published).

[21] G. Savard, J. Phys. **312**, 052004 (2011).

[22] F. Herfurth *et al.*, Nucl. Instrum. Methods Phys. Res., Sect. A **469**, 254 (2001).

[23] T. Mariner and W. Bleakney, Rev. Sci. Instrum. **20**, 297 (1949).

[24] G. W. Monk and G. K. Werner, Rev. Sci. Instrum. **20**, 93 (1949).

[25] C. F. Robinson and L. G. Hall, Rev. Sci. Instrum. **27**, 504 (1956).

[26] K. Yano and S. H. Be, Jpn. J. Appl. Phys. **19**, 1019 (1980).

[27] W. Bleakney and J. A. Hipple, Phys. Rev. **53**, 521 (1938).

[28] A. Borschevsky, L. F. Pasteka, V. Pershina, E. Eliav, and U. Kaldor, Phys. Rev. A **91**, 020501(R) (2015).

[29] Yu. Ts. Oganessian *et al.*, Phys. Rev. C **87**, 014302 (2013).

[30] U. Forsberg *et al.*, Nucl. Phys. **A953**, 117 (2016).